# Bounding Performance and Suppressing Intercarrier Interference in Wireless Mobile OFDM

Xiaodong Cai, *Member, IEEE,* and Georgios B. Giannakis, *Fellow, IEEE*

***Abstract*—While rapid variations of the fading channel cause intercarrier interference (ICI) in orthogonal frequency-division multiplexing (OFDM), thereby degrading its performance considerably, they also introduce temporal diversity, which can be exploited to improve the performance. In this paper, we first derive a matched-filter bound (MFB) for OFDM transmissions over doubly selective Rayleigh fading channels, which benchmarks the best possible performance if ICI is completely canceled without noise enhancement. We then derive universal performance bounds which show that the time-varying channel causes most of the symbol energy to be distributed over a few subcarriers, and that the ICI power on a subcarrier mainly comes from several neighboring subcarriers. Based on this fact, we develop low-complexity minimum mean-square error and decision-feedback equalizer (DFE) receivers for ICI suppression. Simulations show that the DFE receiver can collect significant gains of ICI-impaired OFDM with affordable complexity. In the relatively low Doppler frequency region, bit-error rate of the DFE receiver is close to the MFB.**

***Index Terms*—Doubly selective Rayleigh fading, interference suppression, orthogonal frequency-division multiplexing (OFDM).**

## I. Introduction

ORTHOGONAL frequency-division multiplexing (OFDM) is a promising transmission modality to achieve high data rates over wireless mobile channels [32]. In OFDM, the available channel bandwidth is divided into $N$ overlapping narrowband subchannels. The serial high-rate data stream is converted into $N$ parallel low-rate substreams, which are modulated onto $N$ subcarriers corresponding to the $N$ narrowband subchannels. A cyclic prefix is inserted before each transmitted data block. If the length of the cyclic prefix is equal to, or longer than, the delay spread of the channel, intersymbol interference (ISI) is completely eliminated by design. For time-invariant frequency-selective multipath channels, a simple one-tap equalizer can be employed to recover the transmitted symbol on each subcarrier.

Paper approved by C. Tellambura, the Editor for Modulation and Signal Design of the IEEE Communications Society. Manuscript received July 18, 2002; revised July 7, 2003. This work was supported through collaborative participation in the Communications and Networks Consortium, sponsored by the U.S. Army Research Laboratory under the Collaborative Technology Alliance Program, under Cooperative Agreement DAAD19-01-2-0011. The U.S. Government is authorized to reproduce and distribute reprints for Government purposes notwithstanding any copyright notation thereon. This paper was presented in part at the 36th Asilomar Conference on Signals, Systems, and Computers, Pacific Grove, CA, November 3–6, 2002.

The authors are with the Department of Electrical and Computer Engineering, University of Minnesota, Minneapolis, MN 55455 USA (e-mail: caixd@ece.umn.edu; georgios@ece.umn.edu).

Digital Object Identifier 10.1109/TCOMM.2003.820752

In wireless environments, however, the multipath channel is time varying because of the user's mobility. Channel variations may also arise due to the presence of an unknown carrier frequency offset (CFO). While subcarriers in OFDM are orthogonal in the presence of a time-invariant channel, rapid channel variations over a symbol period destroy the orthogonality among subcarriers, and result in intercarrier interference (ICI) [14], [23], [24]. Since ICI may degrade the bit-error rate (BER) performance severely [20], [28], ICI suppression has received considerable attention. By mapping symbols to a group of subcarriers, self-cancellation schemes have been proposed [1], [27], [29], [33] to render OFDM transmissions less sensitive to the CFO-induced ICI, at the price of sacrificing some bandwidth. Since CFO can be estimated accurately [19], the CFO-induced ICI can also be canceled efficiently by compensating for CFO effects at the receiver. While suppression of the CFO-induced ICI is relatively easy to implement, it is more challenging to cancel the ICI caused by the Doppler spread of the time-varying fading channel. The exact formulas of and upper bounds on the average ICI power were derived in [14], [23], and [24] for doubly selective fading channels; and an error floor on symbol-error rate (SER) was observed in [24]. In [16], a minimum mean-square error (MMSE) equalizer was developed to suppress ICI, based on a polynomial model of the time-varying channel [4]. The ICI suppression scheme in [12] is only applicable to slowly time-varying channels, since a first-order polynomial channel model was adopted. A linear MMSE equalizer and a successive interference cancellation (SIC) scheme with optimal ordering were advocated in [7]. Since the number of subcarriers $N$ is usually very large, e.g., $N = 1512$ or 6048 in digital video broadcasting (DVB) [26], even the linear MMSE equalizer proposed in [7] demands very high computation, and it may not be feasible in a practical system.

In this paper, we first derive a matched-filter bound (MFB) for OFDM over doubly selective channels. The MFB for frequency-selective fading channels has been extensively studied [8], [15], [18] in order to benchmark the best possible performance that a communication system can achieve over a given channel. The MFB for single-carrier modulation over doubly selective fading channels was investigated in [2], while the MFB for OFDM in a time-selective, frequency-flat Rayleigh fading channel was evaluated in [5]. Our MFB here reveals that the diversity enabled by narrowband OFDM transmissions over a doubly selective fading channel comes from the channel's time selectivity, not from the frequency selectivity, as expected. We then study the symbol energy leakage, and ICI effects due to the Doppler spread. We will show that most of the symbol en-

ergy is leaked from each subcarrier to a few neighboring subcarriers, and most of the ICI on each subcarrier comes from several neighboring subcarriers. Based on this observation, we will develop a low-complexity MMSE equalizer. While the MMSE equalizer still exhibits an error floor on BER, a low-complexity decision-feedback equalizer (DFE) will be derived to collect the diversity, and bring the overall system performance closer to the MFB.

The rest of the paper is organized as follows. Section II presents the signal model and the MFB. Section III studies the symbol energy leakage, and the ICI due to the Doppler spread. The low-complexity MMSE equalizer and the DFE equalizer are developed in Section IV. Simulations are provided in Section V, and Section VI summarizes our conclusions.

*Notation:* Superscripts $T$, $*$, and $\mathcal{H}$ stand for transpose, conjugate, Hermitian transpose, respectively; and $E[]$ denotes expectation with the random variables within the brackets, and $z = y \bmod x$ yields the smallest $z \geq 0$ so that $y = nx+z$ for a nonnegative integer $n$. Column vectors (matrices) are denoted by boldface lowercase (uppercase) letters. We will use $\mathbf{I}_N$ to denote the $N \times N$ identity matrix, $\boldsymbol{\mathcal{D}}(\mathbf{x})$ to denote a diagonal matrix with $\mathbf{x}$ on its diagonal, $[\mathbf{A}]_{m,n}$ to denote the $(m, n)$th entry of the matrix $\mathbf{A}$, and $[\mathbf{x}]_m$ to denote the $m$th entry of the vector $\mathbf{x}$. The matrix $[\mathbf{F}_N]_{m,n} := N^{-1/2}\exp(-j2\pi(m-1)(n-1)/N)$ stands for the $N \times N$ discrete fast Fourier transform (FFT) matrix, and $\mathbf{f}_m$ denotes the $m$th column of $\mathbf{F}_N$. We will use Matlab notation $\mathbf{A}(m:n,:)(\mathbf{A}(:,m:n))$ to extract the submatrix from row (column) $m$ to row (column) $n$, $\mathbf{A}(\mathbf{r},\mathbf{c})$ to extract a submatrix within $\mathbf{A}$ defined by the index vector of desired rows in $\mathbf{r}$, and the index vector of desired columns in $\mathbf{c}$, $\mathbf{x}(m:n)$ to extract entry $m$ to entry $n$, and $\mathbf{x}(\mathbf{r})$ to extract entries defined by the index vector $\mathbf{r}$.

## II. Signal Model and MFB

### A. Continuous Signal Model

Suppose the symbol duration after serial-to-parallel (S/P) conversion is $T_s$; the baseband carrier frequency for the $k$th subcarrier is then $f_k = k/T_s$, $k \in [0, N-1]$, where $N$ denotes the total number of subcarriers. The entire signal bandwidth is $W = N/T_s$. The transmitted signal over a block, including the cyclic prefix, is given by

$$u(t) = T_s^{-\frac{1}{2}} \sum_{k=0}^{N-1} s_k e^{\frac{j2\pi kt}{T_s}}, \quad -T_p \leq t < T_s \tag{1}$$

where $s_k$ is the information-bearing symbol on the $k$th subcarrier, and $T_p$ is the length of the cyclic prefix. We see from (1) that $u(t) = u(t+T_s)$, for $t \in [-T_p, 0)$; thus, $u(t)$ for $t \in [-T_p, 0)$ comprises the cyclic prefix. The duration of an OFDM symbol block with cyclic prefix is $T_b = T_p + T_s$. We assume that all symbols have the same energy $\mathcal{E}_s = E[|s_k|^2]$.

The doubly selective fading channel in wireless communications is often modeled as a wide-sense-stationary uncorrelated-scattering (WSSUS) channel [3], [21, p. 762], with the impulse response given by

$$h(t;\tau) = \sum_{d=0}^{D-1} h(t;\tau_d)\delta(\tau - \tau_d) \tag{2}$$

where $\tau_0 < \tau_1 < \ldots < \tau_{D-1}$, and $\delta(\cdot)$ denotes Dirac's delta function. The autocorrelation function of the WSSUS channel is given by $E[h(t;\tau_1)h^*(t+\Delta t;\tau_2)] = \phi_h(\Delta t;\tau_1)\delta(\tau_1 - \tau_2)$ [3], [21, p. 762]. In a rich-scattering environment, the angle of arrival of the received signal waveform is a uniformly distributed random variable, which implies that the channel's autocorrelation function is separable in time and delay [11], [25]: $\phi_h(\Delta t;\tau) = \phi_t(\Delta t)\phi_\tau(\tau)$, where $\phi_\tau(\tau)$ is the multipath intensity profile [21, p. 762]. The Fourier transform of the time-correlation function $\phi_t(\Delta t)$ is the Doppler power spectrum, which is denoted by $\varphi(f)$. We assume the following.

*AS1:* $\phi_t(\Delta t) = \phi_t(-\Delta t)$, $\varphi(f) = \varphi(-f)$, $\int_{-f_d}^{f_d} \varphi(f)df = 1$, and $\varphi(f) = 0$, for $|f| > f_d$, where $f_d$ is the maximum Doppler frequency.

The classic time-correlation function based on the Jakes' model is $\phi_t(\Delta t) = J_0(2\pi f_d \Delta t)$ [11], where $J_0(x)$ is the zeroth-order Bessel function of the first kind; and, for the uniform Doppler spectrum, we have $\phi_t(\Delta t) = \mathrm{sinc}(2f_d\Delta t)$, where $\mathrm{sinc}(x) = \sin(\pi x)/\pi x$. In the Rayleigh fading channel, $h(t;\tau_d)$ is complex Gaussian with zero mean and variance $\sigma_d^2 := \phi_\tau(\tau_d)$, and $\{h(t;\tau_d)\}_{d=0}^{D-1}$ are independent. The channel is assumed to be normalized, i.e., $\sum_{d=0}^{D-1}\sigma_d^2 = 1$. If $\mathbf{h}(t) := [h(t;\tau_0), \ldots, h(t;\tau_{D-1})]^T$, the covariance matrix of $\mathbf{h}(t)$ is then $\boldsymbol{\Phi}_\tau := \mathrm{diag}(\sigma_0^2, \ldots, \sigma_{D-1}^2)$.

By selecting the cyclic prefix duration $T_p \geq \tau_{D-1}$, the received signal after removing the cyclic prefix is given by $r(t) = x(t) + w(t)$, $0 \leq t < T_s$, where [c.f. (1), (2)]

$$\begin{aligned} x(t) &= \int_{-\infty}^{\infty} h(t;\tau)u(t-\tau)d\tau \\ &= T_s^{-\frac{1}{2}} \sum_{k=0}^{N-1}\sum_{d=0}^{D-1} s_k h(t;\tau_d) e^{-\frac{j2\pi k\tau_d}{T_s}} e^{\frac{j2\pi kt}{T_s}} \end{aligned} \tag{3}$$

and $w(t)$ is complex additive white Gaussian noise (AWGN) with zero mean, and two-sided power spectral density $N_0/2$ per dimension. The demodulated signal on the $m$th subcarrier is given by

$$y_m = T_s^{-\frac{1}{2}} \int_0^{T_s} r(t)e^{-\frac{j2\pi mt}{T_s}}dt = \tilde{x}_m + \tilde{w}_m \tag{4}$$

where $\tilde{w}_m$ is a complex Gaussian random variable with zero mean and variance $N_0/2$ per dimension, and

$$\begin{aligned} \tilde{x}_m &= T_s^{-\frac{1}{2}} \int_0^{T_s} x(t)e^{-\frac{j2\pi mt}{T_s}}dt \\ &= \frac{1}{T_s}\sum_{k=0}^{N-1}\sum_{d=0}^{D-1}\left[s_k e^{-\frac{j2\pi k\tau_d}{T_s}} \int_0^{T_s} h(t;\tau_d)e^{-\frac{j2\pi(m-k)t}{T_s}}dt\right]. \end{aligned} \tag{5}$$

Since $\int_0^{T_s} e^{-j2\pi(m-k)t/T_s}dt = T_s\delta(m-k)$, we deduce from (5) that the ICI is absent if $h(t;\tau_d)$ is constant $\forall d$ over a symbol period.

### B. Discrete Signal Model

Denote the chip duration by $T_c := T_s/N$, and select $T_p$ so that $N_p := T_p/T_c$ is an integer. Sampling the continuous signal

in (1) at $t_n = nT_c$, the normalized discrete transmitted signal becomes

$$u(n) := u(nT_c) = \frac{1}{\sqrt{N}} \sum_{k=0}^{N-1} s_k e^{\frac{j2\pi kn}{N}}, \quad n \in [-N_p, N-1]. \tag{6}$$

Let $P = N + N_p$, $\mathbf{u} := [u(-N_p), \ldots, u(N-1)]^T$, $\mathbf{s} := [s_0, \ldots, s_{N-1}]^T$, and $\mathbf{T}_{cp} := [\mathbf{I}_{cp}^T, \mathbf{I}_N]^T$, where $\mathbf{I}_{cp}$ is the matrix formed by the last $N_p$ rows of the identity matrix $\mathbf{I}_N$. The $P \times 1$ transmitted signal vector $\mathbf{u}$ can be expressed in a compact form as $\mathbf{u} = \mathbf{T}_{cp}\mathbf{F}_N^{\mathcal{H}}\mathbf{s}$. From this expression, we see that the discrete transmitted block $\mathbf{u}$ can be obtained efficiently by performing inverse fast Fourier transform (IFFT) on the symbol vectors.

Since the signal bandwidth is limited to $W$, the WSSUS channel in (2) can also be modeled as a tapped delay line (TDL) with random taps [3], [21, p. 762]. The delay between two consecutive taps is $T_c = 1/W$, and the channel coefficients at the $l$th tap are given by [3], [30]

$$\begin{aligned} c(t;l) &= \int_{-\infty}^{\infty} h(t;\tau)\mathrm{sinc}\left(\frac{\tau}{T_c} - l\right) d\tau \\ &= \sum_{d=0}^{D-1} h(t;\tau_d)\mathrm{sinc}\left(\frac{\tau_d}{T_c} - l\right), \quad l \in [0, L] \end{aligned} \tag{7}$$

where $L = \lfloor \tau_{D-1}/T_c \rfloor + 1$. Let the discrete channel coefficients be $h_d(n;l) := c(nT_c;l)$ and $\mathbf{h}_d(n) := [h_d(n;0), \ldots, h_d(n;L)]^T$. Defining $[\mathbf{G}]_{l+1,d+1} := \mathrm{sinc}(\tau_d/T_c - l)$, $l \in [0, L]$, $d \in [0, D-1]$, we have $\mathbf{h}_d(n) = \mathbf{G}\mathbf{h}(nT_c)$. The covariance of $\mathbf{h}_d(n)$ is expressed as $\mathbf{R}_{h_d} = \mathbf{G}\mathbf{\Phi}_\tau\mathbf{G}^{\mathcal{H}}$. We see that the TDL channel coefficients $\mathbf{h}_d(n)$ are generally correlated, unless $\tau_d$ is a multiple of $T_c \forall d$, so that $\mathbf{G}$ is diagonal.

Since $N_p \geq L$, the discrete received signal after removing the cyclic prefix is given by $r(n) = x(n) + w(n)$, $n \in [0, N-1]$, where

$$x(n) = \sum_{l=0}^{L} h_d(n;l)u(n-l), \quad n \in [0, N-1] \tag{8}$$

and $w(n)$ is a complex Gaussian random variable with zero mean and variance $N_0/2$ per dimension. Let the channel frequency response on the $k$th subcarrier, at time $nT_c$, be $H(n;k) := \sum_{l=0}^{L} h_d(n;l)\exp(-j2\pi kl/N) = \tilde{\mathbf{f}}_k^T\mathbf{h}_d(n)$, where $\tilde{\mathbf{f}}_k := \sqrt{N}\mathbf{f}_k(1:L+1)$. Let $\mathbf{x} = [x(0), \ldots, x(N-1)]^T$, and $\tilde{\mathbf{h}}_k = [H(0;k), \ldots, H(N-1;k)]^T$. Substituting (6) into (8), we obtain $\mathbf{x} = \sum_{k=0}^{N-1} \boldsymbol{\mathcal{D}}(\mathbf{f}_k^*)\tilde{\mathbf{h}}_k s_k$, and the received signal vector $\mathbf{r} = [r(0), \ldots, r(N-1)]^T$ can be written as $\mathbf{r} = \mathbf{x} + \mathbf{w}$, where $\mathbf{w} := [w(0), \ldots, w(N-1)]^T$. To demodulate the symbols on different subcarriers, we perform FFT on $\mathbf{r}$, and obtain $\mathbf{y} = \mathbf{F}_N\mathbf{r} = \tilde{\mathbf{x}} + \tilde{\mathbf{w}}$, where $\tilde{\mathbf{x}} = \mathbf{F}_N\mathbf{x}$, and $\tilde{\mathbf{w}}$ is still white Gaussian noise, since the FFT matrix $\mathbf{F}_N$ is unitary. Letting $[\mathbf{A}]_{m,k} := \mathbf{f}_m^T\boldsymbol{\mathcal{D}}(\mathbf{f}_k^*)\tilde{\mathbf{h}}_k$, we have $\tilde{\mathbf{x}} = \mathbf{A}\mathbf{s}$; and $\mathbf{y}$ becomes

$$\mathbf{y} = \mathbf{A}\mathbf{s} + \tilde{\mathbf{w}}. \tag{9}$$

Since $\mathbf{f}_m^T\boldsymbol{\mathcal{D}}(\mathbf{f}_k^*)\mathbf{1} = \delta(m-k)$, the matrix $\mathbf{A}$ is diagonal if all entries of $\tilde{\mathbf{h}}_k$ are equal, where one denotes the vector with all-one entries. Hence, if the channel is time invariant over a block, there is no ICI.

### C. MFB

To derive an MFB, we suppose that only one subcarrier, say subcarrier $k$, is used to transmit every symbol. The received block $\mathbf{y}$ in (9) then becomes

$$\mathbf{y} = \mathbf{F}_N\boldsymbol{\mathcal{D}}(\mathbf{f}_k^*)\tilde{\mathbf{h}}_k s_k + \tilde{\mathbf{w}}. \tag{10}$$

The matched-filter output is written as $z = \tilde{\mathbf{h}}_k^{\mathcal{H}}\boldsymbol{\mathcal{D}}(\mathbf{f}_k)\mathbf{F}_N^{\mathcal{H}}\mathbf{y} = N^{-1}\tilde{\mathbf{h}}_k^{\mathcal{H}}\tilde{\mathbf{h}}_k s_k + \nu$, where $\nu$ is Gaussian noise with zero mean, and variance $N^{-1}\tilde{\mathbf{h}}_k^{\mathcal{H}}\tilde{\mathbf{h}}_k N_0$. Defining the time-correlation matrix as $[\mathbf{\Phi}_t]_{m,n} := \phi_t(|m-n|T_c)$, and $\eta_k := (\tilde{\mathbf{f}}_k^T\mathbf{R}_{h_d}\tilde{\mathbf{f}}_k)^{1/2}$, we can write the covariance matrix of $\tilde{\mathbf{h}}_k$ as $\mathbf{R}_{\tilde{h}_k} = E[\tilde{\mathbf{h}}_k\tilde{\mathbf{h}}_k^{\mathcal{H}}] = \eta_k^2\mathbf{\Phi}_t$. Suppose that the rank of $\mathbf{\Phi}_t$ is $r$, and the $r$ nonzero eigenvalues are $\lambda_i$, $i \in [1, r]$. Then, $z$ can be expressed as $z = \sum_{i=1}^{r}\gamma_i|\breve{h}_i|^2 s_k + \nu$, where $\breve{h}_i$, $i \in [1, r]$ are zero-mean complex Gaussian random variables with unit variance, and $\gamma_i := \eta_k^2\lambda_i/N$. If all eigenvalues $\lambda_i, i \in [1, r]$ are distinct, the BER for binary phase-shift keying (BPSK) and quaternary phase-shift keying (QPSK) can be found as [15]

$$P_e = \frac{1}{2}\sum_{i=1}^{r}\mu_i\left[1 - \sqrt{\frac{\mathcal{E}_b\gamma_i}{(\mathcal{E}_b\gamma_i + N_0)}}\right] \tag{11}$$

where $\mu_i := \prod_{j=1, j\neq i}^{r}\gamma_i/(\gamma_i - \gamma_j)$, $\mathcal{E}_b = \mathcal{E}_s$ for BPSK, and $\mathcal{E}_b = \mathcal{E}_s/2$ for QPSK. When some eigenvalues are identical, the BER can also be found, as in [15].

*Remark 1:* If the channel is fixed in a symbol period, the entries of $\mathbf{\Phi}_t$ are all ones, and thus $r = 1$; but when the channel is rapidly varying, the rank of the Hermitian matrix $\mathbf{\Phi}_t$ will be $r > 1$. This confirms the temporal diversity that becomes available with channel variations. We also verify that different from wideband signaling schemes [2], OFDM loses the diversity introduced by the frequency selectivity of the multipath channel.

*Remark 2:* Since *AS1* implies that $\phi_t(0) = 1$, and $\mathrm{Tr}(\mathbf{\Phi}_t) = N$, we deduce from (10) that the average received power of $s_k$ is $\mathcal{P}_k = \mathrm{Tr}(\mathbf{R}_{h_d})/N = \eta_k^2\mathcal{E}_s$, where Tr() denotes the trace of the matrix in parentheses. If the TDL channel taps are uncorrelated, i.e., $\mathbf{G}$ is diagonal, then $\mathcal{P}_k = \mathcal{E}_s\sum_{d=0}^{D-1}\sigma_d^2 = \mathcal{E}_s, \forall k$; and thus, all subcarriers have the same average received power. However, when the channel taps are correlated, the average received powers on different subcarriers are unequal. This fact is true in both time-selective and time-flat fading channels. Fig. 1 shows the empirical probability distribution function (pdf) of the normalized average received power $\mathcal{P}_k/\mathcal{E}_s$. The number of subcarriers is $N = 128$, and the TDL channel is generated from a two-tap WSSUS channel using (7). The delay of the first tap of the WSSUS channel is zero, and the delay of the second tap is uniformly distributed in $(0, NT_c/8]$. The empirical pdf is obtained by 10 000 independent channel realizations. In Fig. 1, the solid line is the empirical pdf of powers on all subcarriers. We see that although the variations of the average received power are not severe, different subcarriers do have different power distributions.

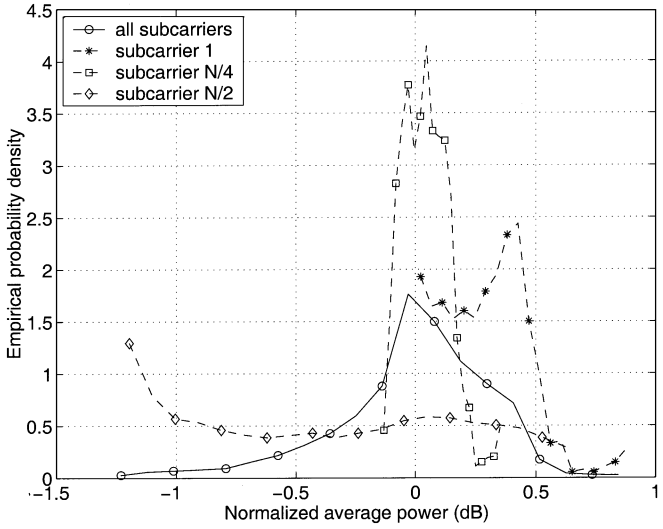


Fig. 1. Empirical pdf of the normalized average received power for correlated channels.

## III. Symbol Energy Distribution and ICI

### A. Symbol Energy Distribution and ICI for the Discrete Signal Model

The energy of $s_k$ leaked to the $m$th subcarrier can be found as

$$\psi_{m,k} = \mathcal{E}_s E\left[\left|[\mathbf{A}]_{m,k}\right|^2\right] = \mathcal{P}_k \mathbf{f}_m^T \boldsymbol{\mathcal{D}}\left(\mathbf{f}_k^*\right) \boldsymbol{\Phi}_t \boldsymbol{\mathcal{D}}(\mathbf{f}_k) \mathbf{f}_m^* \quad (12)$$

where $\mathcal{P}_k = \eta_k^2 \mathcal{E}_s$ is the average received power of $s_k$. Since $[\boldsymbol{\Phi}_t]_{m,n} = \phi_t(|m-n|T_c)$, (12) becomes

$$\psi_{m,k} = \mathcal{P}_k N^{-2} \left\{ N + 2\sum_{n=1}^{N-1} (N-n)\phi_t(nT_c) \times \cos\left[\frac{2\pi(m-k)n}{N}\right] \right\}. \quad (13)$$

The total ICI power on the $m$th subcarrier is written as $\mathcal{P}_I^{(m)} = \sum_{\substack{k=0 \\ k\neq m}}^{N-1} \psi_{m,k}$. As we discussed in *Remark 2*, when the TDL channel taps are uncorrelated, $\mathcal{P}_k = \mathcal{E}_s$, $\forall k$. In this case, $\mathcal{P}_I^{(m)} = \mathcal{P}_I$, $\forall m$, where $\mathcal{P}_I$ is given by [24]

$$\mathcal{P}_I = \mathcal{E}_s N^{-2} \sum_{\substack{k=0 \\ k\neq m}}^{N-1} \left\{ N + 2\sum_{n=1}^{N-1} (N-n)\phi_t(nT_c) \times \cos\left[\frac{2\pi(m-k)n}{N}\right] \right\}. \quad (14)$$

When $\mathcal{P}_k = \mathcal{E}_s$, $\forall k$, the total ICI power is equal to the symbol energy leaking to all other subcarriers; thus, we have

$$\mathcal{P}_I = \mathcal{E}_s - \psi_{k,k} = \mathcal{E}_s \left\{ 1 - \frac{\left[N + 2\sum_{n=1}^{N-1}(N-n)\phi_t(nT_c)\right]}{N^2} \right\}. \quad (15)$$

Note that (15) can also be obtained from (14) using the formula $\sum_{k=0}^{N-1} \cos[2\pi(m-k)n/N] = 0$. While (13) and (15) can be evaluated numerically, they do not provide insights regarding the symbol energy leakage and ICI. This motivates us to study the symbol energy leakage, and the resulting ICI based on the continuous signal model. We shall see later that the symbol energy leakage derived from the continuous signal model is almost the same as that from the discrete signal model, when the number of subcarriers $N$ is moderately large.

### B. Lower Bound on Partial Energy Distribution for the Continuous Signal Model

From (5), the signal component of $s_k$ on the $m$th subcarrier is given by

$$\tilde{x}_{m,k} = \frac{s_k}{T_s} \sum_{d=0}^{D-1} e^{-\frac{j2\pi m\tau_d}{T_s}} \int_0^{T_s} h(t;\tau_d) e^{-\frac{j2\pi(m-k)t}{T_s}} dt. \quad (16)$$

Since $h(t;\tau_d)$, $d \in [0, D-1]$, are uncorrelated, the energy of $s_k$ on the $m$th subcarrier, $\psi_q = E[|\tilde{x}_{m,k}|^2]$, can be written as

$$\psi_q = \frac{\mathcal{E}_s}{T_s^2} \sum_{d=0}^{D-1} \int_0^{T_s}\int_0^{T_s} \sigma_l^2 \phi_t(t_1-t_2) e^{-j2\pi q(t_1-t_2)} dt_1 dt_2 = \frac{\mathcal{E}_s}{T_s^2} \int_0^{T_s}\int_0^{T_s} \phi_t(t_1-t_2) e^{-j2\pi q(t_1-t_2)} dt_1 dt_2 \quad (17)$$

where $q = m-k$. Comparing (12) with (17), we see that if $\mathcal{P}_k = \mathcal{E}_s$, and $N$ is large, $\psi_{m,k}$ in (12) is approximately equal to $\psi_q$ in (17), since the integration in (17) is replaced by its numerical approximation in (12). Thus, our analysis based on the continuous model also provides insight regarding the symbol energy leakage of digital OFDM transmissions. While $\psi_{m,k}$ in (13) may depend on the subcarrier index $k$, if the TDL channel taps are correlated, $\psi_q$ in continuous signal model is the same for all subcarriers. Under *AS1*, (17) can be simplified as [14]

$$\psi_q = \mathcal{E}_s \int_{-1}^{1} \phi_t(T_s x)\left(1-|x|\right) e^{-j2\pi qx} dx. \quad (18)$$

Using the identity $\sum_{q=-\infty}^{\infty} e^{-j2\pi qx} = \sum_{m=-\infty}^{\infty} \delta(x-m)$ [22, p. 60], we obtain the average received power of $s_k$ as $\mathcal{P}_k = \sum_{q=-\infty}^{\infty} \psi_q = \mathcal{E}_s$. Unlike the discrete signal model, $\mathcal{P}_k$ in the continuous signal model is the same for all $k$'s; thus, the average received power on each subcarrier is identical.

Under *AS1*, the time-correlation function can also be written as $\phi_t(\Delta t) = 2\int_0^1 \varphi_n(f)\cos(2\pi f_d \Delta t f) df$, where $\varphi_n(f) := f_d \varphi(f_d f)$, $0 \le f \le 1$, and $2\int_0^1 \varphi_n(f) df = 1$ is the normalized Doppler spectrum. Plugging $\phi_t(\Delta t)$ into (18), we have

$$\psi_q = 4\mathcal{E}_s \int_0^1\int_0^1 \varphi_n(f)\cos(2\pi f_d T_s f x)\cos(2\pi q x)(1-x) dx df. \quad (19)$$

Integrating with respect to $x$, (19) reduces to

$$\psi_q = \pi^{-2}\mathcal{E}_s \int_0^1 \varphi_n(f)\sin^2(\pi f_d T_s f) \times \left[\frac{1}{(f_d T_s f + q)^2} + \frac{1}{(f_d T_s f - q)^2}\right] df. \quad (20)$$

Using (20), the energy of $s_k$ distributed to subcarriers $k-Q$ to $k+Q$ can be expressed as

$$\Psi_Q = \sum_{q=-Q}^{Q} \psi_q = 2\mathcal{E}_s \int_0^1 \varphi_n(f)\zeta_Q(f) df \quad (21)$$

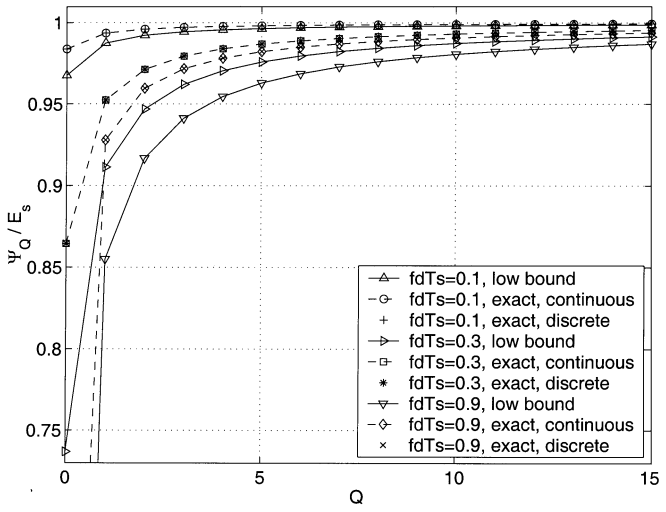


Fig. 2. Normalized symbol energy distribution.

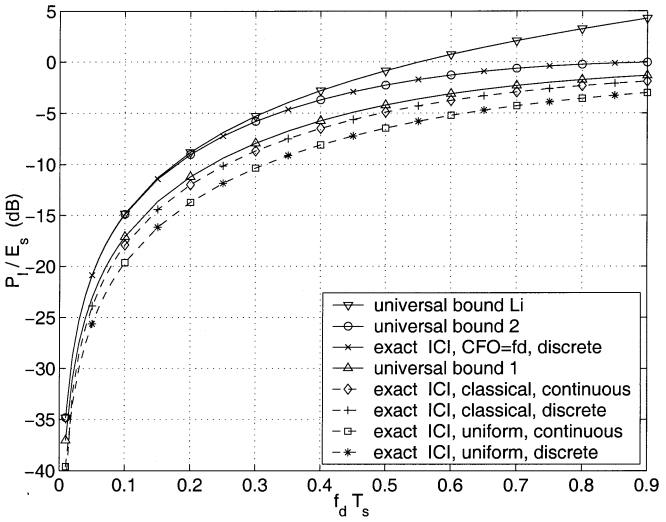


Fig. 3. Comparison of exact total ICI power and universal upper bounds.

where

$$\zeta_Q(f) := \pi^{-2}\sin^2(\pi f_d T_s f) \times \left[(f_d T_s f)^{-2} + \sum_{q=1}^{Q}(f_d T_s f + q)^{-2} + (f_d T_s f - q)^{-2}\right]. \tag{22}$$

Since $\varphi_n(f) \geq 0$, $2\int_0^1 \varphi_n(f)df = 1$, extending the convex combination inequality [10, p. 535] to the integral case, we obtain a universal lower bound on $\Psi_q/\mathcal{E}_s$ as

$$\frac{\Psi_Q}{\mathcal{E}_s} \geq \min \zeta_Q(f), \quad 0 \leq f \leq 1 \tag{23}$$

and the normalized Doppler spectrum achieving this lower bound is $\varphi_n(f) = [\delta(f - f_{lb}/f_d) + \delta(f + f_{lb}/f_d)]/2$, where $f_{lb} = \arg_f \min \zeta_Q(f)$, $0 \leq f \leq 1$. An upper bound on $\Psi_Q/\mathcal{E}_s$ can also be derived by applying the Cauchy–Schwartz inequality [9, p. 1054] to (21). This bound can be used to check the tightness of the lower bound (23). However, since it is not pertinent to our investigation of the total ICI power or the ICI suppression schemes developed in Section IV, we will not derive this upper bound.

The exact normalized symbol energy distribution $\Psi_q/\mathcal{P}_k$, and its lower bound given in (23), are depicted in Fig. 2 for different normalized Doppler frequencies $f_d T_s$. The Jakes' Doppler spectrum is used for calculating the exact symbol energy distribution. In the discrete signal model, the number of subcarriers is $N = 128$. We see that the results for the discrete signal model match well those of the continuous signal model. When $f_d T_s = 0.1$, more than 98% of the $s_k$'s energy is distributed on the $k$th subcarrier, and its two neighboring subcarriers. If the Doppler frequency increases, more symbol energy leaks to neighboring subcarriers. When $f_d T_s = 0.9$, more than 95% of the symbol energy is spread over nine subcarriers.

### C. Upper Bound on Total ICI for the Continuous Signal Model

The ICI power for finite $N$ has no significant difference from that for infinite $N$ [14]; thus, we assume that $N$ is infinite in the ICI analysis in this and the next subsection. Since $\mathcal{P}_k = \mathcal{E}_s, \forall k$, in the case of infinite subcarriers, the ICI power on the $k$th subcarrier is equal to the power of $s_k$ leaking to other subcarriers, which can be found as

$$\mathcal{P}_I = \mathcal{E}_s - \psi_0 = 2\mathcal{E}_s \int_0^1 \varphi_n(f)\left[1 - \operatorname{sinc}^2(f_d T_s f)\right] df. \tag{24}$$

For the continuous Doppler spectrum induced by mobility, a universal upper bound on ICI can be found by applying the Cauchy–Schwartz inequality to (24) as

$$\mathcal{P}_I^{(\mathrm{ub1})} = \frac{\mathcal{E}_s \int_0^1 \left[1 - \operatorname{sinc}^2(f_d T_s f)\right]^2 df}{\int_0^1 \left[1 - \operatorname{sinc}^2(f_d T_s f)\right] df} \tag{25}$$

and the normalized Doppler spectrum achieving this upper bound is $\varphi_n(f) = ((1 - \operatorname{sinc}^2(f_d T_s f))/(2\int_0^1[1 - \operatorname{sinc}^2(f_d T_s f)]dt))$.

If the ICI is caused by an unknown CFO, $f_{\mathrm{CFO}}$, which can be viewed as a random variable in $[0, f_d]$, the conditional normalized Doppler spectrum is $\varphi_n(f) = [\delta(f - f_{\mathrm{CFO}}/f_d) + \delta(f + f_{\mathrm{CFO}}/f_d)]/2$. If $f_d T_s < 1$, then $\mathcal{P}_I$ is maximized when $f_{\mathrm{CFO}} = f_d$, since $\operatorname{sinc}^2(f_d T_s f)$ is a decreasing nonnegative function for $f \in [0, 1]$; thus, an upper bound on $\mathcal{P}_I$ can be written as

$$\mathcal{P}_I^{(\mathrm{ub2})} = \begin{cases} \mathcal{E}_s\left[1 - \operatorname{sinc}^2(f_d T_s)\right], & f_d T_s < 1 \\ \mathcal{E}_s, & f_d T_s \geq 1. \end{cases} \tag{26}$$

The exact normalized ICI power for the Jakes' and uniform Doppler spectra, along with the upper bounds (25) and (26), are displayed in Fig. 3. The exact ICI power in the discrete signal model is calculated from (15) using $N = 128$; and (24) is used to compute the ICI power in the continuous signal model. We see that the ICI power in the discrete signal model matches very well that of the continuous signal model with an infinite number of subcarriers. The universal upper bound in [14], denoted by universal bound Li, is also shown in the figure. It is seen that our universal bounds are much tighter than the bound given in [14]. Comparing the universal bounds (25) and (26) reveals that for a given maximum Doppler frequency $f_d$, the largest ICI power is caused by a deterministic carrier frequency offset at $f_{\mathrm{CFO}} = f_d$.

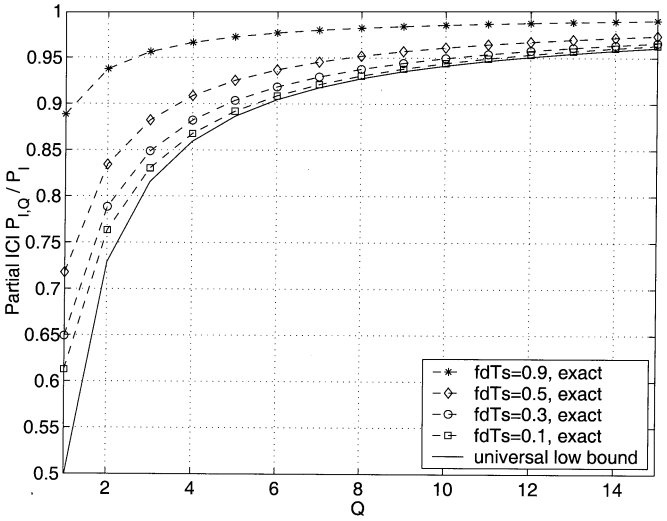


Fig. 4. Comparison of exact partial ICI power and the universal lower bound.

### D. Lower Bound on Partial ICI for the Continuous Signal Model

The ICI on the $k$th subcarrier from the subcarriers $k-1$ to $k-Q$, and $k+1$ to $k+Q$, is $P_{I,Q} = 2\sum_{q=1}^{Q}\psi_q$. In the following, we shall derive a lower bound on $P_{I,Q}/\mathcal{P}_I$, when $f_dT_s < 1$. Let $\xi_q := 1/(f_dT_sf+q)^2 + 1/(f_dT_sf-q)^2 = 2[q^2+(f_dT_sf)^2]/[q^2-(f_dT_sf)^2]^2$. Since $0 \le f_dT_sf < 1$, we have $\xi_q \ge 2/q^2$, and $\xi_q < 2(q^2+1)/(q^2-1)^2 = (q-1)^{-2} + (q+1)^{-2}$, $q > 1$. From (20), we have

$$P_{I,Q} \ge 4\varepsilon\sum_{q=1}^{Q}\frac{1}{q^2} = 4\varepsilon S(Q) \tag{27}$$

where $\varepsilon := \pi^{-2}\mathcal{E}_s\int_0^1\varphi_n(f)\sin^2(\pi f_dT_sf)df$, $S(Q) = \sum_{q=1}^{Q}1/q^2$, $Q = 1,2,\ldots$, and $S(0) = 0$. Defining $\bar{P}_{I,Q} := \mathcal{P}_I - P_{I,Q} = 2\sum_{q=Q+1}^{\infty}\psi_q$, we obtain

$$\bar{P}_{I,Q} < 2\varepsilon\sum_{q=Q+1}^{\infty}\left[(q-1)^{-2}+(q+1)^{-2}\right], \quad Q > 0. \tag{28}$$

Since $\sum_{q=1}^{\infty}1/q^2 = \pi^2/6$ [9, p. 8], (28) becomes

$$\bar{P}_{I,Q} < 2\varepsilon\left[\frac{\pi^2}{3} - S(Q-1) - S(Q+1)\right]. \tag{29}$$

Combining (27) and (29), we have

$$\frac{P_{I,Q}}{\bar{P}_{I,Q}} > \frac{2S(Q)}{\frac{\pi^2}{3} - S(Q-1) - S(Q+1)} =: \vartheta. \tag{30}$$

A universal lower bound on the normalized partial ICI, $P_{I,Q}$, is then found from (30) as

$$\frac{P_{I,Q}}{\mathcal{P}_I} \ge \frac{\vartheta}{(1+\vartheta)}. \tag{31}$$

This universal bound does not depend on the Doppler spectrum, and the maximum Doppler frequency $f_d$, as long as $f_dT_s < 1$ is satisfied. The exact $P_{I,Q}/\mathcal{P}_I$ for the Jakes' Doppler spectrum and the universal lower bound are depicted in Fig. 4. From the lower bound in Fig. 4, we observe that more than 90% of the ICI power comes from 12 neighboring subcarriers. While the exact ICI is very close to the lower bound when the maximum Doppler frequency is low, it is far above the lower bound when the maximum Doppler frequency is high. This is somewhat surprising, since as we discussed before, there is more energy leakage when the maximum Doppler frequency is high. However, since Fig. 4 shows the partial ICI power normalized by the total ICI power, it is possible that when the maximum Doppler frequency is high, the subcarriers close to the subcarrier of interest contribute a high percentage to the total ICI power.

## IV. ICI Suppression

MMSE and SIC receivers were developed in [7] for suppressing ICI in OFDM based on all FFT output samples. Since the number of subcarriers $N$ is usually very large, these receivers have very high complexity. In this section, we will exploit the fact that most of a symbol's energy is distributed to a few subcarriers, and the ICI on a subcarrier mainly comes from several neighboring subcarriers to develop low-complexity MMSE and DFE receivers.

### A. Low-Complexity MMSE ICI Suppression

Suppose we are interested in detecting the symbol $s_k$. Let $K = 2Q+1$, and define a $K\times 1$ vector with the $i$th entry $[\boldsymbol{\rho}_k]_i := [(k-Q-1+i) \bmod N]+1$, $i = 1,\ldots,K$. Let $\mathbf{y}_k := \mathbf{y}(\boldsymbol{\rho}_k)$, $\mathbf{A}_k = \mathbf{A}(\boldsymbol{\rho}_k,:)$, and $\tilde{\mathbf{w}}_k = \tilde{\mathbf{w}}(\boldsymbol{\rho}_k)$. From (9), we have

$$\mathbf{y}_k = \mathbf{A}_k\mathbf{s} + \tilde{\mathbf{w}}_k. \tag{32}$$

The MMSE receiver for detecting $s_k$ based on (32) is $\mathbf{m}_k = \mathbf{R}_k^{-1}\mathbf{p}_k$, where $\mathbf{R}_k = E[\mathbf{y}_k\mathbf{y}_k^{\mathcal{H}}] = \mathcal{E}_s\mathbf{A}_k\mathbf{A}_k^{\mathcal{H}} + N_0\mathbf{I}_k$, and $\mathbf{p}_k = \mathbf{A}_k(:,k)$. The parameter $K$ can be chosen to tradeoff between the performance and the complexity. According to our analysis in Section IV, we can select $K \ll N$, while still being able to suppress ICI effectively. To detect $N$ symbols, we should find $N$ MMSE receivers $\mathbf{m}_k$, $k\in[0,N-1]$. The major computation involved for each $k$ is in calculating the covariance matrix $\mathbf{R}_k$ and its inverse. Since the first $K-1$ rows of $\mathbf{R}_{k+1}$ are the same as the last $K-1$ rows of $\mathbf{R}_k$, we can recursively calculate the inverse of $\mathbf{R}_k$, which greatly reduces complexity.

If we partition $\mathbf{A}_k$ into $\mathbf{A}_k = [\mathbf{a}_k \;\; \bar{\mathbf{A}}_k^{\mathcal{H}}]^{\mathcal{H}}$, then $\mathbf{R}_k$ can be written as

$$\mathbf{R}_k = \begin{bmatrix}\theta_k & \boldsymbol{\theta}_k^{\mathcal{H}} \\ \boldsymbol{\theta}_k & \boldsymbol{\Theta}_k\end{bmatrix} \tag{33}$$

where $\theta_k := \mathcal{E}_s\mathbf{a}_k^{\mathcal{H}}\mathbf{a}_k + N_0$, $\boldsymbol{\theta}_k := \mathcal{E}_s\bar{\mathbf{A}}_k\mathbf{a}_k$, and $\boldsymbol{\Theta}_k := \mathcal{E}_s\bar{\mathbf{A}}_k\bar{\mathbf{A}}_k^{\mathcal{H}} + N_0\mathbf{I}_{K-1}$. Let the inverse of $\mathbf{R}_k$ be

$$\mathbf{R}_k^{-1} = \begin{bmatrix}v_{k,11} & \mathbf{v}_{k,21}^{\mathcal{H}} \\ \mathbf{v}_{k,21} & \mathbf{V}_{k,22}\end{bmatrix} \tag{34}$$

where $v_{k,11}$ is a scalar, $\mathbf{v}_{k,12}$ is a $(K-1)\times 1$ vector, and $\mathbf{V}_{k,22}$ is a $(K-1)\times(K-1)$ matrix. In the Appendix, we show that

$$\boldsymbol{\Theta}_k^{-1} = \mathbf{V}_{k,22} - \frac{\mathbf{v}_{k,21}\mathbf{v}_{k,21}^{\mathcal{H}}}{v_{k,11}}. \tag{35}$$

If we partition $\mathbf{A}_{k+1}$ into $\mathbf{A}_{k+1} = [\bar{\mathbf{A}}_k^{\mathcal{H}} \;\; \tilde{\mathbf{a}}_{k+1}]^{\mathcal{H}}$, we have

$$\mathbf{R}_{k+1} = \begin{bmatrix}\boldsymbol{\Theta}_k & \tilde{\boldsymbol{\theta}}_{k+1} \\ \tilde{\boldsymbol{\theta}}_{k+1}^{\mathcal{H}} & \tilde{\theta}_{k+1}\end{bmatrix} \tag{36}$$

where $\tilde{\theta}_{k+1} := \mathcal{E}_s \tilde{\mathbf{a}}_{k+1}^{\mathcal{H}} \tilde{\mathbf{a}}_{k+1} + N_0$, and $\tilde{\boldsymbol{\theta}}_{k+1} := \mathcal{E}_s \bar{\mathbf{A}}_k \tilde{\mathbf{a}}_{k+1}$. Let $\beta_{k+1} := (\tilde{\theta}_{k+1} - \tilde{\boldsymbol{\theta}}_{k+1}^{\mathcal{H}} \boldsymbol{\Theta}_k^{-1} \tilde{\boldsymbol{\theta}}_{k+1})^{-1}$, $\mathbf{b}_{k+1} := -\boldsymbol{\Theta}_k^{-1} \tilde{\boldsymbol{\theta}}_{k+1}$. In the Appendix, we prove that

$$\mathbf{R}_{k+1}^{-1} = \begin{bmatrix} \boldsymbol{\Theta}_k^{-1} + \mathbf{b}_{k+1}\mathbf{b}_{k+1}^{\mathcal{H}}\beta_{k+1} & \mathbf{b}_{k+1}\beta_{k+1} \\ \mathbf{b}_{k+1}^{\mathcal{H}}\beta_{k+1} & \beta_{k+1} \end{bmatrix}. \quad (37)$$

Hence, $\mathbf{R}_{k+1}^{-1}$ can be computed from $\mathbf{R}_k^{-1}$ through $\boldsymbol{\Theta}_k^{-1}$, as in (35). While our recursive MMSE receiver is reminiscent of a sequential MMSE estimator [13, p. 392], they are different from each other, since they are derived from two different signal models.

Calculating $\boldsymbol{\Theta}_k^{-1}$, $\mathbf{b}_{k+1}$, and $\beta_{k+1}$ requires $\mathcal{O}(K^2)$, $\mathcal{O}(K^2)$, and $\mathcal{O}(K)$ operations, respectively; the computation of $\tilde{\theta}_{k+1}$ is $\mathcal{O}(N)$, and $\tilde{\boldsymbol{\theta}}_{k+1}$ is $\mathcal{O}(NK)$. Hence, the major computation to obtain $\mathbf{R}_{k+1}^{-1}$ is in calculating $\tilde{\boldsymbol{\theta}}_{k+1}$. To find $\mathbf{R}_0^{-1}$, we need $\mathcal{O}(NK^2)$ operations to calculate $\mathbf{R}_0$, and $\mathcal{O}(K^3)$ operations to invert $\mathbf{R}_0$. Therefore, the total computational complexity for detecting an OFDM block is $\mathcal{O}(N^2K)$. On the other hand, using an MMSE receiver based on the whole block in (9), as suggested in [7], requires $\mathcal{O}(N^3)$ operations. Since $K \ll N$, the computational complexity reduces substantially. While we can decrease $K$ to reduce complexity, the performance may degrade when $K$ is very small. To improve the BER performance while retaining low receiver complexity, we develop a DFE receiver in the next subsection.

### B. Decision Feedback ICI Cancellation

The DFE receiver has well-documented merits for channel equalization and multiuser detection (MUD) [21], [31]. In [31], the DFE MUD for synchronous code-division multiple access (CDMA) over Gaussian channels was investigated systematically, where it was shown that the DFE outperforms the linear detector for every user. Our signal model in (9) is essentially the same as the signal model for synchronous CDMA [31], if we view the symbol $s_k$ coming from a virtual user $k$, and $\mathbf{A}(:, k+1)$ as the spreading code of user $k$. Generally speaking, we can apply any of the DFE options in [31] to the signal model (9). However, it requires a large computation to optimally or suboptimally find the detection order for the DFE receiver [31]. Since our objective here is to develop a low-complexity DEF receiver for ICI suppression in OFDM, we will not pursue any sophisticated ordering.

We first find the symbol with the largest energy by ordering the norm of the columns of $\mathbf{A}$. Suppose that $s_m$ has the largest symbol energy. Starting from the $m$th subcarrier, we detect symbols successively, either in the forward or the backward order. Supposing we detect symbols in the forward order, the detection order is $s_m, \ldots, s_{N-1}, s_0, \ldots, s_{m-1}$. We use an MMSE receiver based on the signal vector $\mathbf{y}_m$ given in (32) to detect the symbol $s_m$. For detecting symbols $s_k$, $k \neq m$, we reconstruct the signal vectors of the previously detected symbols, and then subtract them from the received signal vector $\mathbf{y}_k$. Letting $\hat{s}_m$ denote the detected symbol of $s_m$, and $[\boldsymbol{\varrho}]_i := (m+i-1) \bmod N$, $i = 1, \ldots, N$, we have $\tilde{\mathbf{y}}_k := \mathbf{y}_k - \sum_{i=1}^{n_k} A_k(:, [\boldsymbol{\varrho}]_i + 1)\hat{s}_{[\boldsymbol{\varrho}]_i}$, where $k = [\boldsymbol{\varrho}]_2, [\boldsymbol{\varrho}]_3, \ldots, [\boldsymbol{\varrho}]_n$, $n_k = k - m$, $k > m$, or $n_k = N - m + k$, $k < m$. Assume that all previous symbols are detected correctly; i.e., $\hat{s}_{[\boldsymbol{\varrho}]_i} = s_{[\boldsymbol{\varrho}]_i}$, $i \in [1, n_k]$, $\tilde{\mathbf{y}}_k$ is found from (32) as $\tilde{\mathbf{y}}_k = \tilde{\mathbf{a}}_k \tilde{\mathbf{s}}_k + \tilde{\mathbf{w}}_k$, where $\tilde{\mathbf{A}}_k = \mathbf{A}_k(:, \boldsymbol{\varrho}(n_k+1 : N)+\mathbf{1})$, and $\tilde{\mathbf{s}}_k = \mathbf{s}(\boldsymbol{\varrho}(n_k+1 : N)+\mathbf{1})$. If we also rearrange the columns of $\mathbf{A}_m$ to obtain $\tilde{\mathbf{A}}_m = \mathbf{A}_m(:, \boldsymbol{\varrho} + \mathbf{1})$, the first $K-1$ rows of $\tilde{\mathbf{A}}_{k+1}$ are the same as the last $K-1$ rows of $\tilde{\mathbf{A}}_k$, except that the first column of $\tilde{\mathbf{A}}_k$ is removed. Based on this fact, we can modify the recursive method in the previous subsection to find the MMSE DFE receiver for $s_k$.

We partition the matrix $\tilde{\mathbf{A}}_k$ in the same manner as we partitioned $\mathbf{A}_k$. With slightly misusing the notation, we still denote the covariance matrix of $\tilde{\mathbf{y}}_k$ as $\mathbf{R}_k$, which is partitioned in (33). Now, we write $\tilde{\mathbf{A}}_{k+1}$ as $\tilde{\mathbf{A}}_{k+1} = [\mathbf{B}_{k+1}^{\mathcal{H}} \;\; \tilde{\mathbf{a}}_{k+1}]^{\mathcal{H}}$, where $\mathbf{B}_{k+1} = \bar{\mathbf{A}}_k(:, 2 : N-n_k)$. Note that the $(K-1)\times(N-n_k-1)$ matrix $\mathbf{B}_{k+1}$ contains the last $N - n_k - 1$ columns of the $(K-1)\times(N-n_k)$ matrix $\bar{\mathbf{A}}_k$. The covariance matrix of $\tilde{\mathbf{y}}_{k+1}$, $\mathbf{R}_{k+1}$, is expressed as

$$\mathbf{R}_{k+1} = \begin{bmatrix} \tilde{\boldsymbol{\Theta}}_{k+1} & \tilde{\boldsymbol{\theta}}_{k+1} \\ \tilde{\boldsymbol{\theta}}_{k+1}^{\mathcal{H}} & \tilde{\theta}_{k+1} \end{bmatrix} \quad (38)$$

where $\tilde{\boldsymbol{\Theta}}_{k+1} := \mathcal{E}_s \mathbf{B}_{k+1}\mathbf{B}_{k+1}^{\mathcal{H}} + N_0 \mathbf{I}_{K-1}$, $\tilde{\theta}_{k+1} := \mathcal{E}_s \tilde{\mathbf{a}}_{k+1}^{\mathcal{H}} \tilde{\mathbf{a}}_{k+1} + N_0$, and $\tilde{\boldsymbol{\theta}}_{k+1} := \mathcal{E}_s \mathbf{B}_{k+1} \tilde{\mathbf{a}}_{k+1}$. Letting $\boldsymbol{\alpha}_k := \bar{\mathbf{A}}_k(:, 1)$, we have $\tilde{\boldsymbol{\Theta}}_{k+1} = \boldsymbol{\Theta}_k - \mathcal{E}_s \boldsymbol{\alpha}_k \boldsymbol{\alpha}_k^{\mathcal{H}}$. The inverse of $\tilde{\boldsymbol{\Theta}}_{k+1}$ can be found using the matrix inversion lemma [10, p. 19] as

$$\tilde{\boldsymbol{\Theta}}_{k+1}^{-1} = \boldsymbol{\Theta}_k^{-1} + \frac{\left(\boldsymbol{\Theta}_k^{-1}\boldsymbol{\alpha}_k\right)\left(\boldsymbol{\Theta}_k^{-1}\boldsymbol{\alpha}_k\right)^{\mathcal{H}}}{\left(\mathcal{E}_s^{-1} - \boldsymbol{\alpha}_k^{\mathcal{H}}\boldsymbol{\Theta}_k^{-1}\boldsymbol{\alpha}_k\right)}. \quad (39)$$

Letting $\beta_{k+1} := (\tilde{\theta}_{k+1} - \tilde{\boldsymbol{\theta}}_{k+1}^{\mathcal{H}} \tilde{\boldsymbol{\Theta}}_{k+1}^{-1} \tilde{\boldsymbol{\theta}}_{k+1})^{-1}$, and $\mathbf{b}_{k+1} := -\tilde{\boldsymbol{\Theta}}_{k+1}^{-1} \tilde{\boldsymbol{\theta}}_{k+1}$, we can compute $\mathbf{R}_{k+1}^{-1}$ from (37) by replacing $\boldsymbol{\Theta}_k^{-1}$ with $\tilde{\boldsymbol{\Theta}}_{k+1}^{-1}$. The major computation to find $\mathbf{R}_{k+1}^{-1}$ is in calculating $\tilde{\boldsymbol{\theta}}_{k+1}$, which requires $\mathcal{O}((K-1)(N-n_k))$, where $k = [\boldsymbol{\varrho}]_{n_k}$, and $n_k = 1, \ldots, N-1$. Since $\sum_{n=1}^{N} n = N(N-1)/2$, the complexity of the DFE receiver is $\mathcal{O}(N^2K)$, which is in the same order as that of the MMSE receiver.

After the MMSE DFE receiver makes tentative decisions on $N$ symbols, we can use parallel interference cancellation (PIC) to further improve the BER performance. Specifically, letting $\hat{\mathbf{y}}_k := \mathbf{y}_k - \sum_{m=0, m\neq k}^{N-1} \mathbf{A}_k(:, m+1)\hat{s}_m$, the decision variable for $s_k$ is $z_k = \mathbf{A}_k^{\mathcal{H}}(:, k+1)\hat{\mathbf{y}}_k$. This PIC procedure may iterate more than once to enhance the BER performance. Since each PIC iteration requires $\mathcal{O}(N^2)$ operations, using PIC iterations here will not significantly increase the complexity relative to the original MMSE DFE, which requires $\mathcal{O}(N^2K)$ operations.

### C. Channel Estimation

The MMSE and DFE receivers require channel state information (CSI). If we use pilot tones to estimate the time-varying channel, the channel estimator itself suffers from ICI. Here, we multiplex pilot symbols with the OFDM blocks in the time domain to facilitate channel estimation, as proposed in [7]. It was shown in [6] that when the space between two consecutive pilot symbol blocks is less than $1/(2f_d)$, the MMSE channel estimator incurs a very small estimation error; and the BER degradation using the estimated CSI is negligible. If we insert a pilot symbol block of length $T_{\rm ps}$ every $N_{\rm ps}$ OFDM blocks, then we should choose $N_{\rm ps}$ and $T_{\rm ps}$ such that $N_{\rm ps}T_b + T_{\rm ps} < 1/(2f_d)$. On the other hand, once $N_{\rm ps}$ and $T_{\rm ps}$ have been selected, the normalized Doppler frequency should be $f_dT_s <$

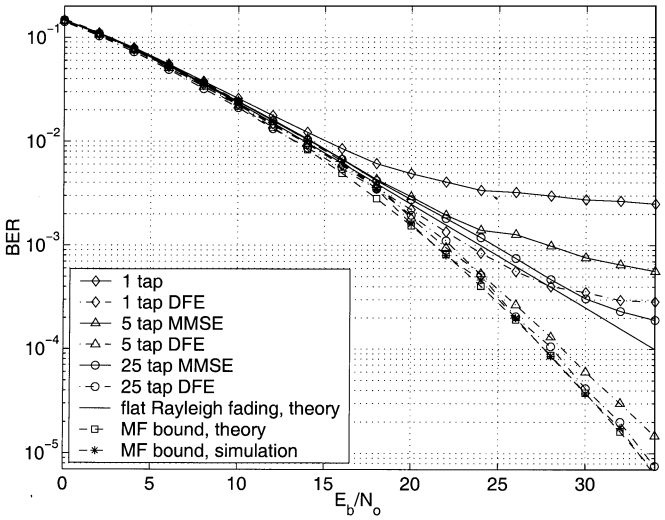


Fig. 5. BER comparison, uncorrelated channel, perfect CSI, $f_dT_s = 0.05$.

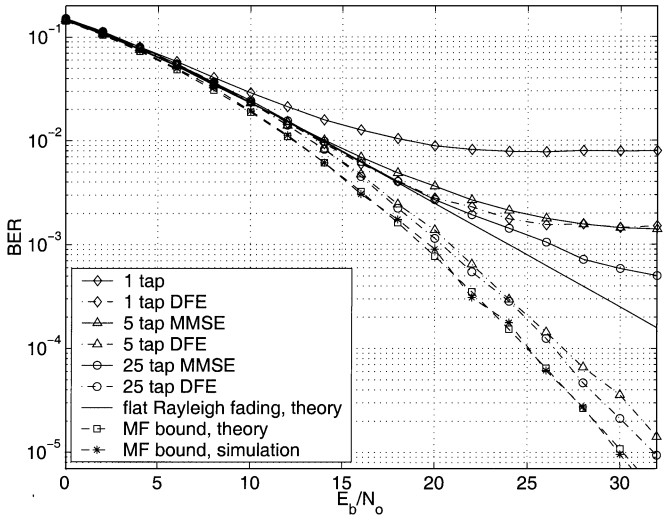


Fig. 6. BER comparison, uncorrelated channel, perfect CSI, $f_dT_s = 0.1$.

$T_s/[2(N_{\rm ps}T_b + T_{\rm ps})]$. If the system is required to operate when $f_dT_s \geq T_s/[2(N_{\rm ps}T_b + T_{\rm ps})]$, we need to consider alternative channel estimators, or we should jointly design the transmitter and receiver as in [17] to collect the temporal diversity without suffering from ICI.

## V. Simulations

In this section, we test the MMSE and DFE ICI suppression schemes via computer simulations based on the discrete signal model. The number of subcarriers is chosen to be $N = 128$, and the length of the cyclic prefix is $N_p = N/8$. QPSK constellation is adopted, with bit energy $\mathcal{E}_b = \mathcal{E}_s/2$. We simulate a two-tap WSSUS channel with an exponential multipath intensity profile, i.e., $\sigma_d^2 = \exp(-d/D)/\sum_{d=0}^{D-1}\sigma_d^2$, $D = 2$, and $d = 0, 1$. Each channel tap is a complex Gaussian random process independently generated with the Jakes' Doppler spectrum. The delay of the first tap is zero. In the uncorrelated channel case, the delay of the second tap is generated from the set $\{T_c, 2T_c, \ldots, N_pT_c\}$ with equal probability; in the correlated channel case, the delay of the second tap is uniformly distributed in $(0, N_pT_c]$, and the

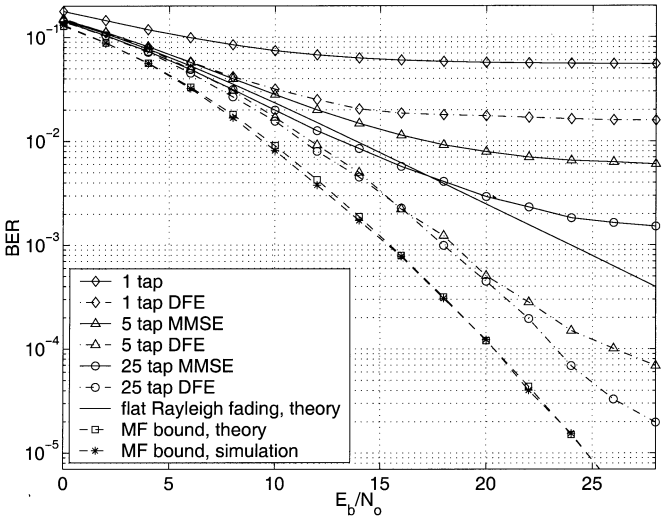


Fig. 7. BER comparison, uncorrelated channel, perfect CSI, $f_dT_s = 0.3$.

TDL channel taps are then generated using (7). In the DFE detection, we use two iterations.

*Test Case 1 (uncorrelated channel and perfect CSI)*: Figs. 5–7 compare the BER performance of the MMSE and DFE equalizers for different Doppler frequencies. The theoretical BER for the flat Rayleigh fading channel, the theoretical MFB calculated from (11), and the simulated MFB are also displayed in these figures. From the MFB, we see that the time variations of the channel introduce temporal diversity, which increases as the Doppler frequency becomes large. While the BER performance of the MMSE equalizer improves as the number of the equalizer taps $K$ increases, it still exhibits an error floor at high $\mathcal{E}_b/N_0$. The DFE equalizer outperforms the MMSE equalizer with the same number of taps. However, the one-tap DFE still has poor performance, even when the Doppler frequency is as low as $f_dT_s = 0.05$. The five-tap DFE equalizer exhibits considerable performance improvement over the one-tap DFE equalizer, and its BER curve is close to that of the 25-tap DFE equalizer. The small gap between the MFB and the BER of the five-tap DFE equalizer shows that we can suppress ICI effectively, and improve the BER performance significantly with a low-complexity DFE equalizer.

*Test Case 2 (correlated channel and perfect CSI)*: As discussed in Section II and shown in Fig. 1, the correlation of the channel taps causes unequal average received power distribution among different subcarriers. In this example, we test the impact of the channel correlation on the BER performance. Comparing Fig. 8 with Fig. 6, we see that BER in the correlated channel is almost the same as that in the uncorrelated channel, which suggests that the channel correlation caused by the bandlimited signaling has no major effect on the BER performance.

*Test Case 3 (uncorrelated channel and estimated CSI)*: In this test, the channel is estimated using pilot symbols, and the BER is shown in Fig. 9 with $f_dT_s = 0.3$. To ensure that the rate of the pilot blocks is higher than $f_d/2$, every OFDM block is followed by a pilot block of length $2T_p$. Notice that we have used the least number of pilot blocks to guarantee the performance of the channel estimator. The throughput loss incurred by the pilot blocks is $2T_p/(T_s + T_p)$. For a given data rate, it is possible that

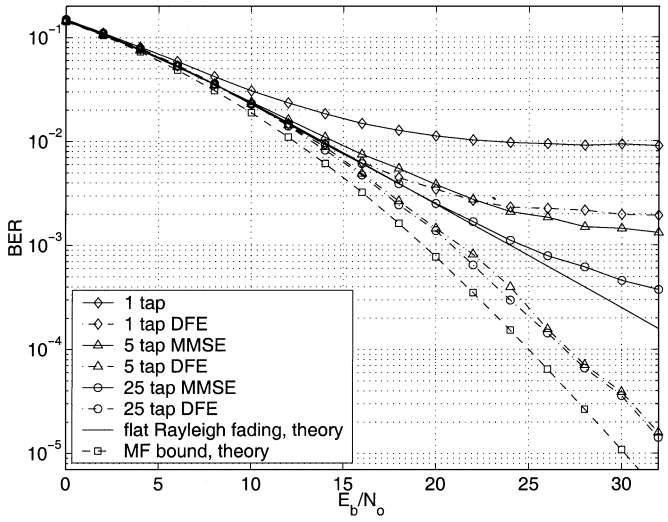


Fig. 8. BER comparison, correlated channel, perfect CSI, $f_dT_s = 0.1$.

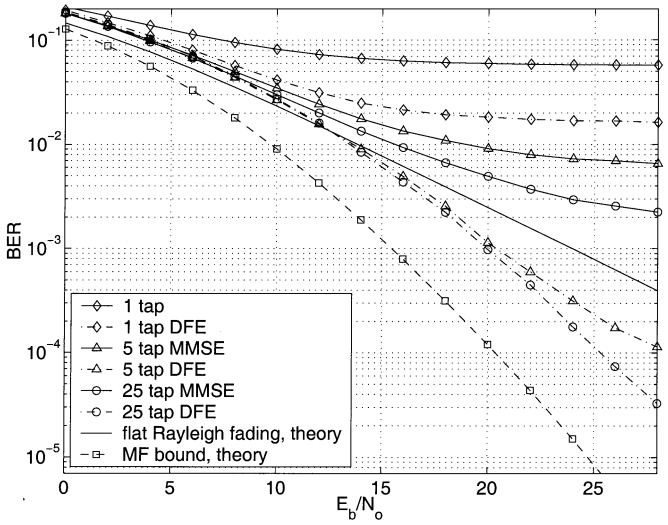


Fig. 9. BER comparison, uncorrelated channel, estimated CSI, $f_dT_s = 0.3$.

$T_s \gg T_p$ if the number of subcarriers is large. In this case, the throughput loss is very small. When the Doppler frequency is low, we can further reduce the number pilot blocks to increase throughput. A 10-tap MMSE filter is employed to estimate the channel [6]. If we compare the BER curves displayed in Fig. 9 and Fig. 7, we see that the channel estimation error results only in slight BER degradation.

## VI. Conclusions

We benchmarked the impact of channel variations on OFDM, by deriving an MFB for doubly selective fading channels. We verified that the channel variations introduce temporal diversity, which has the potential to improve the BER performance if properly exploited. We also studied the ICI and energy leakage that is caused by time-varying mobile channels. Our universal bounds on ICI power reveal that for a given maximum Doppler frequency $f_d$, the maximum ICI power is caused by a carrier frequency offset at $f_d$. A universal lower bound on partial ICI power was derived when $f_dT_s < 1$, which shows that more than 90% of the ICI power comes from 12 neighboring subcarriers. We also showed that most of the symbol energy is distributed over a few subcarriers; e.g., when $f_dT_s = 0.3$, more than 90% of the symbol energy is spread over three subcarriers. These results motivated our development of low-complexity MMSE and DFE receivers for ICI suppression. While the low-complexity MMSE receiver exhibits error floor, the DFE receiver can collect the temporal diversity, and its BER performance comes close to the MFB at relatively low $f_dT_s$. As a by-product of our MFB study, we showed that the channel correlation causes unequal average received power distribution among different subcarriers, and this effect has no significant impact on the BER performance.[1]

## Appendix
## Proof of (35)

Applying the inversion formula for a partitioned matrix [10, p. 18] to $\mathbf{R}_k$ in (33), we obtain

$$\mathbf{V}_{k,22} = \left(\boldsymbol{\Theta}_k - \frac{\boldsymbol{\theta}_k\boldsymbol{\theta}_k^{\mathcal{H}}}{\theta_k}\right)^{-1} \tag{40}$$

$$\mathbf{v}_{k,21} = -\frac{\mathbf{V}_{k,22}\boldsymbol{\theta}_k}{\theta_k} \tag{41}$$

$$v_{k,11} = \left(\theta_k - \boldsymbol{\theta}_k^{\mathcal{H}}\boldsymbol{\Theta}_k^{-1}\boldsymbol{\theta}_k\right)^{-1}. \tag{42}$$

Using the matrix inversion lemma [10, p. 19], we have

$$\mathbf{V}_{k,22} = \boldsymbol{\Theta}_k^{-1} + v_{k,11}\left(\boldsymbol{\Theta}_k^{-1}\boldsymbol{\theta}_k\right)\left(\boldsymbol{\Theta}_k^{-1}\boldsymbol{\theta}_k\right)^{\mathcal{H}}. \tag{43}$$

Plugging (43) into (41), we obtain

$$\mathbf{v}_{k,21} = -v_{k,11}\boldsymbol{\Theta}_k^{-1}\boldsymbol{\theta}_k. \tag{44}$$

Combining (42), (43), and (44), we find $\boldsymbol{\Theta}_k^{-1} = \mathbf{V}_{k,22} - \mathbf{v}_{k,21}\mathbf{v}_{k,21}^{\mathcal{H}}/v_{k,11}$. □

## Proof of (37)

Similar to computing (41)–(43), we can find $\mathbf{R}_{k+1}^{-1}$ given in (37). □

## References

[1] J. Armstrong, "Analysis of new and existing methods of reducing intercarrier interference due to carrier frequency offset in OFDM," *IEEE Trans. Commun.*, vol. 47, pp. 365–369, Mar. 1999.

[2] N. J. Bass and D. P. Taylor, "Matched filter bounds for wireless communication over Rayleigh fading dispersive channels," *IEEE Trans. Commun.*, vol. 49, pp. 1525–1528, Sept. 2001.

[3] P. A. Bello, "Characterization of randomly time-variant linear channels," *IEEE Trans. Commun. Syst.*, vol. COM-11, pp. 360–393, Dec. 1963.

[4] D. K. Borath and B. D. Hart, "Frequency-selective fading channel estimation with a polynomial time-varying channel model," *IEEE Trans. Commun.*, vol. 47, pp. 862–873, June 1999.

[5] W. Burchill and C. Leung, "Matched filter bound for OFDM on Rayleigh fading channels," *Electron. Lett.*, vol. 31, pp. 1716–1717, Sept. 1995.

[6] J. K. Cavers, "An analysis of pilot symbol-assisted modulation for Rayleigh fading channels," *IEEE Trans. Veh. Technol.*, vol. 40, pp. 686–693, Nov. 1991.

[7] Y.-S. Choi, P. J. Voltz, and F. A. Cassara, "On channel estimation and detection for multicarrier signals in fast and selective Rayleigh fading channels," *IEEE Trans. Commun.*, vol. 49, pp. 1375–1387, Aug. 2001.

[1]The views and conclusions contained in this document are those of the authors and should not be interpreted as representing the official policies, either expressed or implied, of the Army Research Laboratory or the U.S. Government.

[8] M. V. Clark, L. J. Greenstein, W. K. Kennedy, and M. Shafi, "Matched filter performance bounds for diversity combing receivers in digital mobile radio," *IEEE Trans. Veh. Technol.*, vol. 41, pp. 356–362, Nov. 1992.
[9] I. S. Gradshtein and I. Ryzhik, *Table of Integrals, Series, and Products*. San Diego, CA: Academic, 2000.
[10] R. A. Horn and C. R. Johnson, *Matrix Analysis*. New York: Cambridge Univ. Press, 1985.
[11] W. C. Jakes, *Microwave Mobile Communications*. New York: Wiley, 1974.
[12] W. G. Jeon, K. H. Chang, and Y. S. Cho, "An equalization technique for orthogonal frequency-division multiplexing systems in time-variant multipath channels," *IEEE Trans. Commun.*, vol. 47, pp. 27–32, Jan. 1999.
[13] S. T. Kay, *Fundamentals of Statistical Signal Processing, Volume I: Estimation Theory*. Englewood Cliffs, NJ: Prentice-Hall, 1993.
[14] Y. G. Li and L. J. Cimini, "Bounds on the interchannel interference of OFDM in time-varying impairments," *IEEE Trans. Commun.*, vol. 49, pp. 401–404, Mar. 2001.
[15] F. Ling, "Matched-filter bound for time-discrete multipath Rayleigh fading channels," *IEEE Trans. Commun.*, vol. 43, pp. 710–713, Feb.–Apr. 1995.
[16] J.-P. M. G. Linnartz and A. Gorokhov, "New equalization approach for OFDM over dispersive and rapidly time-varying channel," in *Proc. PIMRC Conf.*, London, U.K., Sept. 2000, pp. 1375–1379.
[17] X. Ma and G. B. Giannakis, "Maximum-diversity transmissions over doubly selective wireless channels," *IEEE Trans. Inform. Theory*, vol. 49, pp. 1832–1840, July 2003.
[18] J. E. Mazo, "Exact matched-filter bound for two-beam Rayleigh fading," *IEEE Trans. Commun.*, vol. 39, pp. 1027–1030, July 1991.
[19] P. H. Moose, "A technique for orthogonal frequency-division multiplexing frequency offset correction," *IEEE Trans. Commun.*, vol. 42, pp. 2908–2914, Oct. 1994.
[20] T. Pollet, M. V. Bladel, and M. Moeneclaey, "BER sensitivity of OFDM systems to carrier frequency offset and Wiener phase noise," *IEEE Trans. Commun.*, vol. 43, pp. 191–193, Feb.–Apr. 1995.
[21] J. G. Proakis, *Digital Communications*. New York: McGraw-Hill, 1995.
[22] J. G. Proakis and M. Salehi, *Communication Systems Engineering*. Englewood Cliffs, NJ: Prentice-Hall, 1994.
[23] P. Robertson and S. Kaiser, "The effects of Doppler spreads in OFDM(A) mobile radio systems," in *Proc. VTC-Fall*, Amsterdam, The Netherlands, Sept. 1999, pp. 329–333.
[24] M. Russell and G. L. S. Stüber, "Interchannel interference analysis of OFDM in a mobile environment," in *Proc. VTC'95*, Chicago, IL, July 1995, pp. 820–824.
[25] J. S. Sadowsky and V. Kafedxiski, "On the correlation and scattering functions of the WSSUS channel for mobile communications," *IEEE Trans. Veh. Technol.*, vol. 47, pp. 270–282, Feb. 1998.
[26] F. Sanzi and J. Speidel, "An adaptive two-dimensional channel estimation for wireless OFDM with application to mobile DVB-T," *IEEE Trans. Broadcast.*, vol. 46, pp. 128–133, June 2000.
[27] K. Sathananthan and C. Tellambura, "Forward error correction codes to reduce intercarrier interference in OFDM," in *Proc. IEEE Int. Symp. Circuits and Systems*, Sydney, Australia, May 2001, pp. 566–569.
[28] ——, "Probability of error calculation of OFDM systems with frequency offset," *IEEE Trans. Commun.*, vol. 49, pp. 1884–1889, Nov. 2001.
[29] K. A. Seation and J. Armstrong, "Polynomial cancellation coding and finite differences," *IEEE Trans. Inform. Theory*, vol. 46, pp. 311–313, Jan. 2000.
[30] J. Sylora, "Tapped delay line model of linear randomly time-variant WSSUS channel," *Electron. Lett.*, vol. 36, pp. 1656–1657, Sept. 2000.
[31] M. K. Varanasi, "Decision feedback multiuser detection: a systematic approach," *IEEE Trans. Inform. Theory*, vol. 45, pp. 219–240, Jan. 1999.
[32] Z. Wang and G. B. Giannakis, "Wireless multicarrier communications: where Fourier meets Shannon," *IEEE Signal Processing Mag.*, vol. 47, pp. 29–48, May 2000.
[33] Y. Zhao and S. Häggman, "Intercarrier interference self-cancellation scheme for OFDM mobile communication systems," *IEEE Trans. Commun.*, vol. 49, pp. 1185–1191, July 2001.

**Xiaodong Cai** (M'01) received the B.S. degree from Zhejiang University, Hangzhou, China, the M.Eng. degree from the National University of Singapore, Singapore, and the Ph.D. degree from the New Jersey Institute of Technology, Newark, in 2001, all in electrical engineering.

From February 2001 to June 2001, he was a Member of Technical Staff at Lucent Technologies, NJ, working on a WCDMA project; from July 2001 to October 2001, he was a Senior System Engineer at Sony Technology Center, San Diego, CA, involved in developing high-data-rate wireless modems. Since November 2001, he has been a Postdoctoral Research Associate in the Department of Electrical and Computer Engineering, University of Minnesota, Minneapolis. His research interests lie in the areas of communication theory, signal processing, and wireless networks.

**Georgios B. Giannakis** (S'84–M'86–SM'91–F'97) received the Diploma in electrical engineering from the National Technical University of Athens, Greece, in 1981. He received the MSc. degree in electrical engineering in 1983, M.Sc. degree in mathematics in 1986, and the Ph.D. degree in electrical engineering in 1986, from the University of Southern California (USC), Los Angeles.

His general interests span the areas of communications and signal processing, estimation and detection theory, time-series analysis, and system identification, subjects on which he has published more than 150 journal papers, 300 conference papers, and two edited books. Current research focuses on transmitter and receiver diversity techniques for single- and multiuser fading communication channels, comples-field and space–time coding, multicarrier, ultra-wideband wireless communication systems, cross-layer designs, and distributed sensor networks.

Dr. Giannakis is the corecipient of four Best Paper Awards from the IEEE Signal Processing (SP) Society (1992, 1998, 2000, and 2001). He also received the Society's Technical Achievement Award in 2000. He co-organized three IEEE-SP Workshops, and guest co-edited four special issues. He has served as Editor in Chief for the IEEE SIGNAL PROCESSING L ETTERS, as Associate Editor for the IEEE TRANSACTIONS ON SIGNAL PROCESSING and the IEEE SIGNAL PROCESSING LETTERS, as secretary of the SP Conference Board, as member of the SP Publications Board, as member and vice-chair of the Statistical Signal and Array Processing Technical Committee, and as chair of the SP for Communications Technical Committee. He is a member of the Editorial Board for the PROCEEDINGS OF THE IEEE, and the steering committee of the IEEE TRANSACTIONS ON WIRELESS COMMUNICATIONS. He is a member of the IEEE Fellows Election Committee, and the IEEE-SP Society's Board of Governors.